Original article

Validation of a direct method to predict the strength of adhesively bonded joints

U.T.F. Carvalho, R.D.S.G. Campilho *

Departamento de Engenharia Mecânica, Instituto Superior de Engenharia do Porto, Instituto Politécnico do Porto, Rua Dr. António Bernardino de Almeida, 431, 4200-072 Porto, Portugal

Abstract

Cohesive zone models (CZM) are a powerful tool for the design of bonded structures, but they require careful estimation of the cohesive laws for reliable results. This work experimentally evaluates by the *J*-integral/direct method the tensile and shear CZM laws of three adhesives with distinct ductility. Additionally, by the direct method, the precise shape of the cohesive law in tension and shear of the adhesives is defined. The double-cantilever beam (DCB) and end-notched flexure (ENF) specimens were considered to obtain the tensile and shear CZM laws of the adhesives, respectively. After obtaining the tensile and shear CZM laws, triangular, exponential and trapezoidal CZM laws were built to reproduce their behaviour. Validation of these CZM laws was undertaken with a mixed-mode geometry (double-lap joint) considering the same three adhesives and varying overlap lengths (L_O). The strength prediction by this technique revealed accurate predictions for a given CZM law shape, depending on the adhesive ductility, although all CZM law shapes were moderately accurate.

1. Introduction

Currently, significant efforts are being made in the design of aircraft and aeronautical applications to reduce weight and improve reliability. Thus, adhesive bonding techniques have been largely employed, which also enables the combined use of steel with lighter materials such as aluminium or high strength composites. This, in turn, promotes less fuel consumption and reduction in the CO_2 emissions to the atmosphere, consequently bringing a major environment-related advantage [1,2]. Other advantages over mechanical joints are the increase in productivity regarding costs and fabrication times, excellent insulation, superior damping, noise reduction and improved aesthetics [3]. Pethrick [4] recently presented a comprehensive review regarding the adhesives' selection for structural applications. Limitations of bonded joints include the requirement and correct choice of surface treatment to the bonding surfaces, and sensitivity to temperature and humidity [5].

There is a countless number of joint configurations addressed in the literature, although the most common are single-lap, double-lap and scarf joints [6]. The availability of accurate and straight-forward predictive methods is thus mandatory for the safe design of bonded joints.

Although several techniques have been proposed for many decades, beginning with the theoretical analysis of Volkersen [7], the continuum mechanics criteria coupled to a finite element analysis (FEA), linear elastic fracture mechanics (LEFM) or the CZM. CZM been refined ever since were initially proposed some decades ago, to become nowadays a very powerful technique for damage growth and strength prediction of structures, including the analysis of wood failure [8], composite delaminations [9,10] and bonded joint analysis [11,12], for which this technique is particularly suited [13].

While CZM is a powerful technique to predict the strength of bonded joints, some premises must be accounted for to ensure reliable results: the adhesive should be characterized under identical geometrical conditions in which the resulting laws will be used in the simulations, and the stipulated CZM law shape should be consistent with the adhesive's behaviour [14].

* Corresponding author.
E-mail address: raulcampilho@gmail.com (R.D.S.G. Campilho).

Different techniques are nowadays available for the definition of the cohesive parameters (G_{IC}, G_{IIC}, t_n^0 and t_s^0), such as the property identification technique, the direct method and the inverse method. The direct method, which is the purpose of this work, gives the precise shape of the CZM laws of a specific material or interface, since these are estimated from the experimental data of fracture tests such as the DCB or ENF [15]. This is done by differentiation of the tensile strain energy release rate, G_I, for tension, or the shear strain energy release rate, G_{II}, for shear, with respect to the relative opening of the crack (δ_n for tension or δ_s for shear). Nonetheless, it is usual to convert the obtained shape to an approximated parameterized shape for introduction in the FEA software. For an accurate measurement of the required parameters such as δ_n or δ_s, physical sensors [16] or image correlation methods [17,18] can be used. The validity of the direct approach can be checked by numerically replicating the tensile or shear fracture tests with identical dimensions and with the experimentally obtained CZM laws as input for the adhesive layer's behaviour, followed by comparing the obtained P–δ curves with the original ones from the experiments [18]. However, complete validation of the CZM laws should include testing the pure mode CZM laws in a mixed-mode geometry, although to the authors' knowledge such works are not available in the literature, being these works limited to pure-mode verifications.

This work experimentally evaluates by the *J*-integral/direct method the tensile and shear CZM laws of three adhesives with distinct ductility. Additionally, by the direct method, the precise shape of the cohesive law in tension and shear of the adhesives is defined. The DCB and ENF specimens were considered to obtain the tensile and shear CZM laws of the adhesives, respectively. After obtaining the tensile and shear CZM laws, triangular, exponential and trapezoidal CZM laws were built to reproduce their behaviour. Validation of these CZM laws was undertaken with a mixed-mode geometry (double-lap joint) considering the same three adhesives and varying L_O values.

2. Experimental work

2.1. Materials

For the DCB, ENF and double-lap specimens, the high strength and ductile aluminium alloy AA6082 T651 was chosen for the adherends. The tensile mechanical properties of this material were obtained in the work of Campilho et al. [12]. The experimental testing programme included three structural adhesives: the brittle epoxy Araldite® AV138, the ductile epoxy Araldite® 2015 and the ductile polyurethane Sikaforce® 7752. In this manner, different material behaviours are tested. These adhesives were previously characterized regarding the mechanical and toughness properties [12,19,20]. Bulk specimens were tested in a servo-hydraulic machine to obtain Young's modulus (*E*), σ_y, σ_f and ε_f. The DCB test was selected to obtain G_{IC} and the ENF test was used for G_{IIC}. The collected data of the adhesives is summarized in Table 1.

Table 1
Properties of the adhesives Araldite® AV138, Araldite® 2015 and Sikaforce® 7752 [12,19,20].

Property	AV138	2015	7752
Young's modulus, *E* [GPa]	4.9 ± 0.8	1.9 ± 0.2	0.5 ± 0.1
Poisson's ratio, ν	0.35^a	0.33^a	0.30^a
Tensile yield stress, σ_y [MPa]	36.5 ± 2.5	12.6 ± 0.6	3.2 ± 0.5
Tensile failure strength, σ_f [MPa]	39.5 ± 3.2	21.6 ± 1.6	11.5 ± 0.3
Tensile failure strain, ε_f [%]	1.2 ± 0.1	4.8 ± 0.8	19.2 ± 1.4
Shear modulus, *G* [GPa]	1.6 ± 0.01	0.6 ± 0.2	0.2 ± 0.01
Shear yield stress, τ_y [MPa]	25.1 ± 0.3	14.6 ± 1.3	5.2 ± 1.1
Shear failure strength, τ_f [MPa]	30.2 ± 0.4	17.9 ± 1.8	10.2 ± 0.6
Shear failure strain, γ_f [%]	7.8 ± 0.7	43.9 ± 3.4	54.8 ± 6.4
Toughness in tension, G_{IC} [N/mm]	0.20^b	0.4 ± 0.02	2.4 ± 0.2
Toughness in shear, G_{IIC} [N/mm]	0.38^b	4.7 ± 0.3	5.4 ± 0.5

[a] Manufacturer's data.
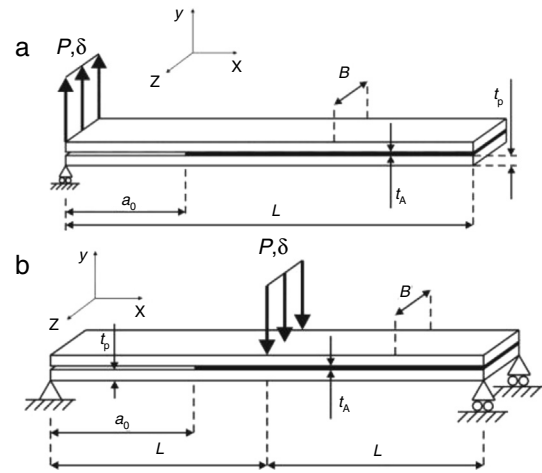[b] Estimated in Campilho et al. [12].

Fig. 1. DCB (a) and ENF (b) specimens for fracture characterization of thin adhesive bonds.
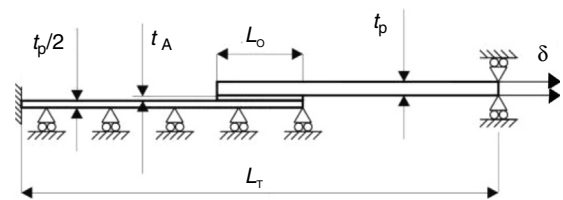

Fig. 2. Double-lap joint specimens for validation of the obtained CZM laws.

2.2. Joint geometries

Fig. 1 shows the geometry and characteristic dimensions of the DCB (a) and ENF specimens (b). The chosen values for the dimensions are: total length $L = 140$ mm (DCB) or mid-span $L = 100$ mm (ENF), initial crack length $a_0 \approx 50$ mm, adherend thickness $t_P = 3$ mm, $t_A = 0.2$ mm and width $B = 25$ mm. Fig. 2 describes the double-lap joints' geometry for validation of the obtained CZM laws, whose dimensions were the following: length between grips $L_T = 170$ mm, $t_P = 3$ mm, $t_A = 0.2$ mm, $L_O = 12.5$, 25, 37.5 and 50 mm and $B = 25$ mm (not represented in the figure).
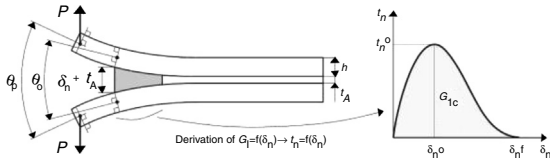
Fig. 3. DCB specimen under loading, with description of the analysis parameters, and estimation of the cohesive law.

Fig. 4. Mesh detail for the $L_O = 25$ mm double-lap joint (CZM failure analysis).

All joint configurations were fabricated and tested at room temperature. Joint tests were carried out in a Shimadzu AG-X 100 electro-mechanical testing machine with a 100 kN load cell. To apply the optical methods used in the DCB and ENF tests, images were recorded by an 18 MPixel digital camera with no zoom and fixed focal distance to approximately 100 mm, which enabled obtaining the values of a, δ_n, δ_s and adherends rotation at the specimen's loading point, θ_o, this last parameter required in the DCB tests for application of the J-integral.

2.3. Direct method for cohesive law estimation

Based on the fundamental expression for J [21], it is possible to derive an expression for G_I (Eq. (1)) applied to the DCB specimen from the concept of energetic force and also the beam theory, as follows [22]

$$G_I = 12\frac{(P_u a)^2}{E_x t_P^3} + P_u \theta_o \quad \text{or} \quad G_I = P_u \theta_p, \tag{1}$$

where P_u represents the applied load per unit width at the adherends' edges and E_x is the adherends' value of E in the longitudinal direction. A schematic representation of δ_n, θ_o and θ_p, required by this method, is given in Fig. 3.

In this figure, δ_n^0 is the relative displacement at t_n^0, and δ_n^f is the tensile failure displacement. The $t_n(\delta_n)$ or tensile CZM law is obtained by differentiation of Eq. (1) with respect to δ_n. More details about this technique applied to the DCB specimen can be found in Ref. [23]. A developed algorithm to measure θ_o and δ_n was used [24], based on digital image correlation and tracking reference points in the scales that follow crack growth during the test.

An identical procedure, i.e., based on the direct method, was used to evaluate G_{IIC} and shear CZM law by the ENF test [22,23], involving the concurrent measurement of the J-integral and δ_s. The G_{II} expression (Eq. (2)) for the ENF specimen gives [25]

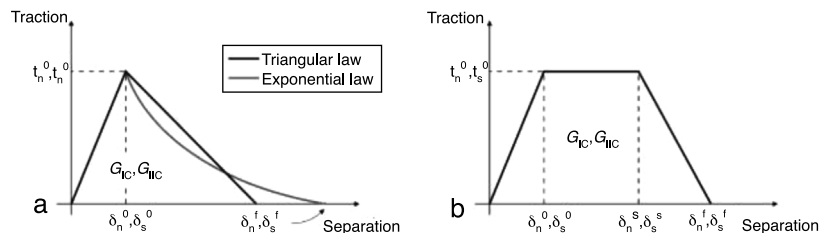$$G_{II} = \frac{9}{16}\frac{(P_u a)^2}{E_x t_P^2} + \frac{3}{8}\frac{P_u \delta_s}{t_P}. \tag{2}$$
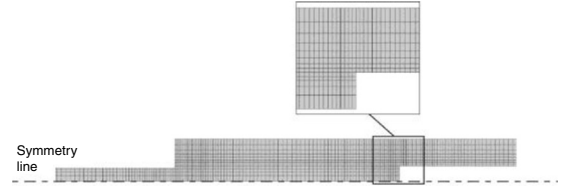
The $t_s-\delta_s$ curve (or shear CZM law) can then be assessed by differentiation of the $G_{II}-\delta_s$ curve. Full details regarding the description of the direct method applied to the ENF specimen, as well as the algorithm to estimate δ_s in every picture of a test, can be found in the work of Leitão et al. [26].

3. Numerical analysis

3.1. Conditions of the numerical analysis

Geometrically non-linear analyses were considered for the double-lap joint models. The adherends were modelled as elasto-plastic continuum bodies and the adhesive was fully represented by a single layer of cohesive elements, i.e., by the continuum CZM approach [19]. The models are two-dimensional, considering CPE4 plane-strain elements of Abaqus®. Apart from this, horizontal symmetry was applied to the double-lap joints. Fig. 4 shows a representative mesh for the CZM strength prediction analysis for a double-lap joint with $L_O = 25$ mm. The FEA mesh included edge grading horizontally from the overlap inner portion towards the overlap edges, and vertically towards the adhesive layer, to increase the simulation speed, although keeping acceptable results. The joints were clamped at one edge and a vertical restraint and tensile displacement was applied at the opposite edge [27].

3.2. CZM implementation in the FEA analysis

CZM are typically founded on a relationship between t_n/t_s and δ_n/δ_s that connects homologous nodes of the cohesive elements, to simulate the elastic behaviour up to t_n^0 (tension) or t_s^0 (shear) and subsequent material degradation up to final failure [28]. In this work, the triangular, trapezoidal and linear-exponential shapes were evaluated to model the tensile and shear behaviour of the adhesive layer. Fig. 5 schematically represents these three CZM shapes with the associated nomenclature for both tensile and shear loadings (δ_s^0 the relative displacement at t_s^0, δ_s^f is the shear failure displacement, and δ_n^s and δ_s^s are the tensile and shear

Fig. 5. CZM laws with triangular, linear-exponential and trapezoidal shapes available in Abaqus®.

stress softening onset displacements of the trapezoidal CZM law, respectively). The definition of δ_n^f and δ_s^f is carried out by making $G_I = G_{IC}$ for tension or $G_{II} = G_{IIC}$ for shear [28].

Due to the unavailability in Abaqus® of mode coupling for the trapezoidal and exponential CZM laws, uncoupled loading modes were considered in all CZM simulations. This is supported by the findings of a previous work [19], in which it was found for composite single-lap joints that the results between mode-coupled and uncoupled predictions are virtually identical.

4. Results

4.1. G_{IC} and G_{IIC} evaluation by the fracture tests

All DCB and ENF specimens revealed a cohesive failure of the adhesive layer. The $G_I-\delta_n$ and $G_{II}-\delta_s$ curves were estimated from the direct method described in Section 2.3 using Eqs. (1) and (2), respectively. Figs. 6 and 7 show typical curves for the three adhesives and the DCB and ENF tests respectively, overlapped by polynomial approximation curves to apply the differentiation procedure leading to the definition of the respective CZM laws.

In agreement with previous works [9], three different stages can be identified in the $G_I-\delta_n$ and $G_{II}-\delta_s$ curves: (1) slow increase of G_I/G_{II} with δ_n/δ_s, (2) steady increase of G_I/G_{II} and (3) the curve tends to a steady-state value of G_I/G_{II}. The different behaviour between the three adhesives is clearly visible. The curves for each adhesive highly differ in terms of G_{IC}/G_{IIC}
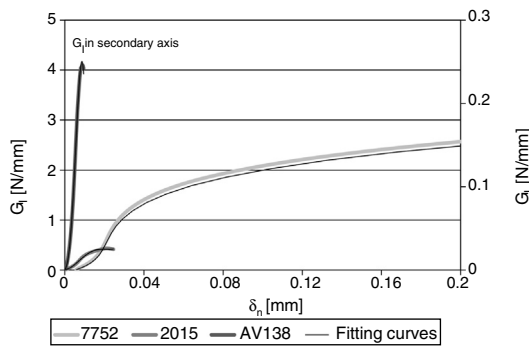
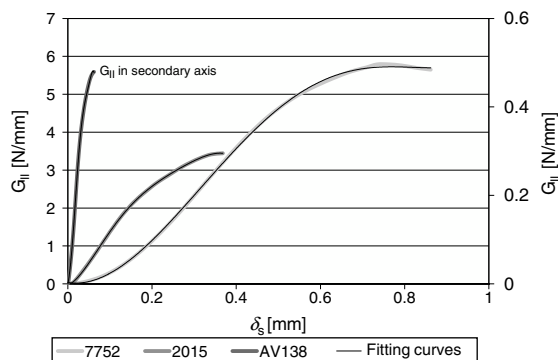Fig. 6. Plot of $G_I-\delta_n$ for a specimen of each tested adhesive: raw curve and polynomial approximations.

Fig. 7. Plot of $G_{II}-\delta_s$ for a specimen of each tested adhesive: raw curve and polynomial approximations.

Table 2
Values of G_{IC} and G_{IIC} [N/mm] for the three adhesives obtained by J-Integral technique [29–31].

Adhesive	Araldite® AV138		Araldite® 2015		Sikaforce® 7752	
Specimen	G_{IC}	G_{IIC}	G_{IC}	G_{IIC}	G_{IC}	G_{IIC}
1	0.224	0.552	0.437	3.444	3.420	–
2	0.252	0.732	0.434	–	3.903	5067
3	0.231	0.676	0.494	2.873	3.842	6050
4	0.329	–	0.456	3.298	4.183	5360
5	0.237	0.566	0.665	3.123	–	6.07
6	0.197	0.533	0.712	3.140	3.502	5173
7	–	0.523	–	3.08	–	5790
8	–	0.479	–	2.901	–	6160
Average	0.245	0.580	0.533	3.123	3.770	5667
Deviation	0.045	0.09	0.123	0.203	0.278	0.459

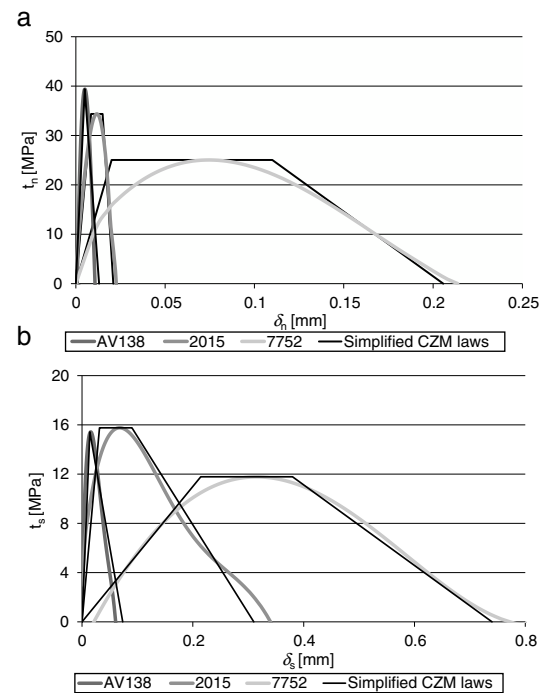Fig. 8. Comparison of representative $t_n-\delta_n$ (a) and $t_s-\delta_s$ (b) curves for each of the adhesives.

measurement and corresponding value of δ_n/δ_s, which corresponds to failure in the CZM law. G_{IC} and G_{IIC} are found by the steady-state values of G_{IC} and G_{IIC} in the respective curve and are attained at crack initiation [16]. Table 2 reviews the G_{IC} and G_{IIC} values obtained by the J-integral for the three adhesives.

Fig. 8 presents a comparison between representative $t_n-\delta_n$ (a) and $t_s-\delta_s$ (b) curves for each of the adhesives (corresponding to the $G_I-\delta_n$ and $G_{II}-\delta_s$ curves of Figs. 6 and 7, respectively). Both tensile and shear CZM laws show that the Araldite® AV138 is best fit by a triangular CZM law because of its brittle behaviour, whilst the Araldite® 2015 and Sikaforce® 7752 are modelled with trapezoidal CZM laws which, in this case, provide the best approximation on account of the plasticization endured after the initial elastic part of the curves. The different behaviour of these three adhesives under tension is consistent with the properties

of the adhesives reported in Table 1, namely ε_f and G_{IC} (tensile CZM laws) and the shear failure strain, ε_f, and G_{IIC} (shear CZM laws). The deviation in the CZM parameters showed a reduced scatter between CZM laws of the same adhesive.

4.2. Strength prediction

The average values of tensile and shear CZM parameters were used to build triangular, trapezoidal and linear-exponential tensile and shear CZM laws for each of the three adhesives. These laws were subsequently input in numerical simulations of double-lap joints respecting the principles depicted in Section 3.1 as a validation of the obtained CZM laws by the *J*-integral/direct method. Fig. 9 compares the experimental and numerical maximum load (P_m) values as function of L_O for the three CZM laws and the adhesives Araldite® AV138 (a), Araldite® 2015 (b) and Sikaforce® 7752.

The comparison between the experiments and CZM predictions by the different law types showed that, for the joints bonded with the Araldite® AV138, the best results are obtained by the tri-

angular CZM law, followed by the trapezoidal CZM law, while the linear-exponential CZM law clearly under estimates P_m. These results are justified by the brittleness of the adhesive, which was attested by the properties depicted in Table 1 and tensile and shear CZM laws represented in Fig. 8. The average absolute error (considering the four L_O values) is 0.56% for the triangular CZM law, 1.17% for the trapezoidal CZM law and 2.79% for the linear-exponential CZM law. The largest % errors always occur for $L_O = 12.5$ mm, disregarding the CZM law type. Differently to this adhesive, for the joints bonded with the Araldite® 2015, the best predictions were attained with the trapezoidal CZM law, which is consistent with the moderate degree of ductility of this adhesive. The triangular and especially the linear-exponential CZM laws under predict the experiments. The average deviations of absolute values, considering all L_O values, are 2.00% (triangular law), 1.03% (trapezoidal law) and 2.76% (linear-exponential law). For this particular adhesive, it was found that, from $L_O = 37.5$ mm, P_m is ruled by the adherends' yielding/tensile net failure rather than the adhesive.

Because of the high ductility of the Sikaforce® 7752, for the joints bonded with this adhesive the trapezoidal CZM law gives the best approximation, while the triangular and linear-exponential CZM laws present identical under predictions. The average % deviations of absolute values of each adhesive are 1.73% (triangular law), 0.36% (trapezoidal law) and 1.73% (linear-exponential law). For $L_O = 50$ mm, P_m is governed by the adherends' yielding or tensile net failure. Globally, for the tested geometrical conditions, no significant errors would be made by using an improper CZM law, i.e., a CZM law that is not the best fit to the tensile and shear CZM laws of the respective adhesive obtained by the direct method. However, this is the result of two factors: (1) the range of L_O values used is this work is relatively limited and (2) for all adhesives, tensile adherend failure or at least adherends plasticization affected the P_m results such that, for the higher P_m values, the joints' failure was no longer ruled by the adhesive but by the adherend's yielding. In fact, in a previous work [19] considering triangular and trapezoidal CZM shapes to model single-lap joints with L_O values up to 80 mm revealed that higher L_O values in joints with non-yielding composite adherends can give differences of over 10% compared to the experiments if the CZM law does not closely follow the adhesive's behaviour. Thus, depending on the required accuracy for the results, the choice of the correct CZM law type may be of importance.

5. Conclusions

The main objective of this work was the assessment of different CZM shapes in predicting the behaviour of a mixed-mode joint geometry bonded with adhesives of distinct ductility, after estimating the tensile and shear CZM laws of the adhesives by the direct method. The DCB and ENF specimens were considered to obtain the tensile and shear CZM laws of the adhesives, respectively. The obtained CZM laws were highly consistent for each loading/adhesive combination. In both loading modes, the Araldite® AV138 was best modelled by a triangular CZM
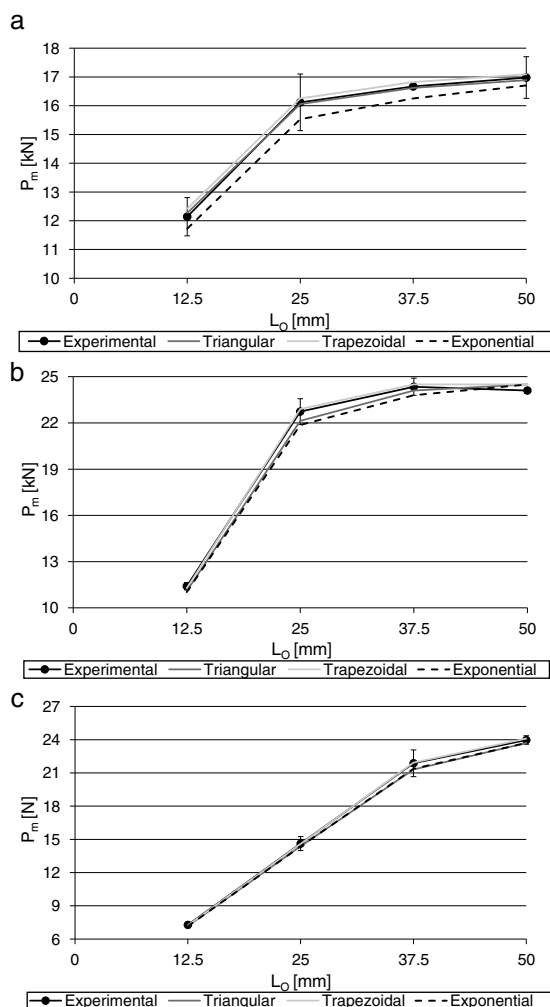
Fig. 9. Comparison between the experimental and numerical P_m values as function of L_O for the three CZM laws and the adhesives Araldite® AV138 (a), Araldite® 2015 (b) and Sikaforce® 7752 (c).

law due to its brittleness, while the ductile Araldite® 2015 and Sikaforce® 7752 showed a better fit with trapezoidal CZM laws. Validation of these CZM laws was undertaken with a mixed-mode geometry (double-lap joint) considering the same three adhesives and varying L_O values. Previous to the analysis, the double-lap joints' strength revealed to be highly dependent on the adhesive type. Actually, the Araldite® AV138 showed a similar P_m value to the Araldite® 2015 for $L_O = 12.5$ mm, but it was unable to increase P_m with L_O by a significant amount on account of being very brittle (oppositely to the Araldite® 2015). The joints bonded with the Sikaforce® 7752 showed a much smaller P_m value for $L_O = 12.5$ mm because of the smaller strengths, but the ductility of this adhesive enabled to increase P_m with L_O in a practically linear relation. All P_m–L_O curves for the three adhesives were affected by the inner adherend's failure or at least plasticization for the higher L_O values. Regarding the P_m comparison between the experiments and numerical predictions, the deviations were small for all CZM laws, although the best results closely followed the previously mentioned agreement regarding the experimental and approximated CZM laws. Thus, for the tested geometrical conditions, no significant errors would be made by using an improper CZM law. However, it should be noted that, depending on the geometry of the joints and adherends' behaviour, the error of using a non-consistent CZM law shape to the behaviour of the adhesive to be simulated can result in non-negligible deviations to the real joints' behaviour.

References

[1] G. Michalos, S. Makris, N. Papakostas, D. Mourtzis, G. Chryssolouris, Automotive assembly technologies review: challenges and outlook for a flexible and adaptive approach, CIRP J. Manuf. Sci. Technol. 2 (2010) 81–91.

[2] M. Goede, M. Stehlin, L. Rafflenbeul, G. Kopp, E. Beeh, Super Light Car—lightweight construction thanks to a multi-material design and function integration, Eur. Transp. Res. Rev. 1 (2008) 5–10.

[3] M.A. Saeimi Sadigh, G. Marami, Investigating the effects of reduced graphene oxide additive on the tensile strength of adhesively bonded joints at different extension rates, Mater. Des. 92 (2016) 36–43.

[4] R.A. Pethrick, Design and ageing of adhesives for structural adhesive bonding – a review, Proc. Inst. Mech. Engrs. Part L J. Mater. Des. Appl. 229 (2015) 349–379.

[5] M. Heshmati, R. Haghani, M. Al-Emrani, Environmental durability of adhesively bonded FRP/steel joints in civil engineering applications: state of the art, Composites Part B Eng. 81 (2015) 259–275.

[6] J. Li, Y. Yan, T. Zhang, Z. Liang, Experimental study of adhesively bonded CFRP joints subjected to tensile loads, Int. J. Adhes. Adhes. 57 (2015) 95–104.

[7] O. Volkersen, Die nietkraftoerteilung in zubeanspruchten nietverbindungen konstanten loschonquerschnitten, Luftfahrtforschung 15 (1938) 41–47.

[8] R.D.S.G. Campilho, M.F.S.F.d. Moura, D.A. Ramantani, J.J.L. Morais, A.M.J.P. Barreto, J.J.M.S. Domingues, Adhesively bonded repair proposal for wood members damaged by horizontal shear using carbon-epoxy patches, J. Adhes. 86 (2010) 649–670.

[9] W.-G. Jiang, S.R. Hallett, B.G. Green, M.R. Wisnom, A concise interface constitutive law for analysis of delamination and splitting in composite materials and its application to scaled notched tensile specimens, Int. J. Numer. Methods Eng. 69 (2007) 1982–1995.

[10] G. Alfano, M.A. Crisfield, Finite element interface models for the delamination analysis of laminated composites: mechanical and computational issues, Int. J. Numer. Methods Eng. 50 (2001) 1701–1736.

[11] V.K. Goyal, E.R. Johnson, V.K. Goyal, Predictive strength-fracture model for composite bonded joints, Compos. Struct. 82 (2008) 434–446.

[12] R.D.S.G. Campilho, M.D. Banea, A.M.G. Pinto, L.F.M. da Silva, A.M.P. de Jesus, Strength prediction of single- and double-lap joints by standard and extended finite element modelling, Int. J. Adhes. Adhes. 31 (2011) 363–372.

[13] T.A.B. Fernandes, R.D.S.G. Campilho, M.D. Banea, L.F.M. da Silva, Adhesive selection for single lap bonded joints: experimentation and advanced techniques for strength prediction, J. Adhes. 91 (2015) 841–862.

[14] R.D.S.G. Campilho, M.F.S.F. de Moura, J.J.M.S. Domingues, Using a cohesive damage model to predict the tensile behaviour of CFRP single-strap repairs, Int. J. Solids Struct. 45 (2008) 1497–1512.

[15] K.C. Pandya, J.G. Williams, Measurement of cohesive zone parameters in tough polyethylene, Polym. Eng. Sci. 40 (2000) 1765–1776.

[16] G. Ji, Z. Ouyang, G. Li, S. Ibekwe, S.S. Pang, Effects of adhesive thickness on global and local Mode-I interfacial fracture of bonded joints, Int. J. Solids Struct. 47 (2010) 2445–2458.

[17] J. Han, T. Siegmund, Cohesive zone model characterization of the adhesive Hysol EA-9394, J. Adhes. Sci. Technol. 26 (2012) 1033–1052.

[18] N. Valoroso, S. Sessa, M. Lepore, G. Cricrì, Identification of mode-I cohesive parameters for bonded interfaces based on DCB test, Eng. Fract. Mech. 104 (2013) 56–79.

[19] R.D.S.G. Campilho, M.D. Banea, J.A.B.P. Neto, L.F.M. da Silva, Modelling adhesive joints with cohesive zone models: effect of the cohesive law shape of the adhesive layer, Int. J. Adhes. Adhes. 44 (2013) 48–56.

[20] T.M.S. Faneco, R.D.S.G. Campilho, F.J.G. da Silva, R.M. Lopes, Strength and fracture characterization of a novel polyurethane adhesive for the automotive industry, J. Testing Eval. 45 (2017) 398–407.

[21] J.R. Rice, A path independent integral and the approximate analysis of strain concentration by notches and cracks, J. Appl. Mech. 35 (1968) 379–386.

[22] Y. Zhu, K.M. Liechti, K. Ravi-Chandar, Direct extraction of rate-dependent traction–separation laws for polyurea/steel interfaces, Int. J. Solids Struct. 46 (2009) 31–51.

[23] R.D.S.G. Campilho, D.C. Moura, D.J.S. Gonçalves, J.F.M.G. da Silva, M.D. Banea, L.F.M. da Silva, Fracture toughness determination of adhesive and co-cured joints in natural fibre composites, Composites Part B Eng. 50 (2013) 120–126.

[24] R.D.S.G. Campilho, D.C. Moura, M.D. Banea, L.F.M. da Silva, Adherend thickness effect on the tensile fracture toughness of a structural adhesive using an optical data acquisition method, Int. J. Adhes. Adhes. 53 (2014) 15–22.

[25] K. Leffler, K.S. Alfredsson, U. Stigh, Shear behaviour of adhesive layers, Int. J. Solids Struct. 44 (2007) 530–545.

[26] A.C.C. Leitão, R.D.S.G. Campilho, D.C. Moura, Shear characterization of adhesive layers by advanced optical techniques, Exp. Mech. 56 (2016) 493–506.

[27] R.D.S.G. Campilho, M.D. Banea, J.A.B.P. Neto, L.F.M. da Silva, Modelling of single-lap joints using cohesive zone models: effect of the cohesive parameters on the output of the simulations, J. Adhes. 88 (2012) 513–533.

[28] A. Turon, C.G. Dávila, P.P. Camanho, J. Costa, An engineering solution for mesh size effects in the simulation of delamination using cohesive zone models, Eng. Fract. Mech. 74 (2007) 1665–1682.

[29] C.J. Constante, R.D.S.G. Campilho, D.C. Moura, Tensile fracture characterization of adhesive joints by standard and optical techniques, Eng. Fract. Mech. 136 (2015) 292–304.

[30] R.D.S.G. Campilho, D.C. Moura, M.D. Banea, L.F.M. da Silva, Adhesive thickness effects of a ductile adhesive by optical measurement techniques, Int. J. Adhes. Adhes. 57 (2015) 125–132.

[31] J.C.S. Azevedo, R.D.S.G. Campilho, J.F.G. da Silva, T.M.S. Faneco, R.M. Lopes, Cohesive law estimation of adhesive joints in mode II condition, Theor. Appl. Fract. Mech. 80 (2015) 143–154.